Engineering electrocatalytic activity in nanosized perovskite cobaltite through surface spin-state transition

Shiming Zhou[1], Xianbing Miao[1], Xu Zhao[1], Chao Ma[1], Yuhao Qiu[2], Zhenpeng Hu[2,3], Jiyin Zhao[1], Lei Shi[1] & Jie Zeng[1]

The activity of electrocatalysts exhibits a strongly dependence on their electronic structures. Specifically, for perovskite oxides, Shao-Horn and co-workers have reported a correlation between the oxygen evolution reaction activity and the e_g orbital occupation of transition-metal ions, which provides guidelines for the design of highly active catalysts. Here we demonstrate a facile method to engineer the e_g filling of perovskite cobaltite $LaCoO_3$ for improving the oxygen evolution reaction activity. By reducing the particle size to $\sim 80\,nm$, the e_g filling of cobalt ions is successfully increased from unity to near the optimal configuration of 1.2 expected by Shao-Horn's principle. Consequently, the activity is significantly enhanced, comparable to those of recently reported cobalt oxides with $e_g^{\sim 1.2}$ configurations. This enhancement is ascribed to the emergence of spin-state transition from low-spin to high-spin states for cobalt ions at the surface of the nanoparticles, leading to more active sites with increased reactivity.

[1] Hefei National Laboratory for Physics Sciences at the Microscale, Hefei Science Center, University of Science and Technology of China, Hefei, Anhui 230026, China. [2] School of Physics, Nankai University, Tianjin 300071, China. [3] State Key Laboratory of Luminescent Materials and Devices, South China University of Technology, Guangzhou 510640, China. Correspondence and requests for materials should be addressed to S.Z. (email: zhousm@ustc.edu.cn) or to Z.H. (email: zphu@nankai.edu.cn) or to J.Z. (email: zengj@ustc.edu.cn).

Electrochemical water splitting is regarded as a prime approach for renewable energy conversion and storage[1,2]. One of the critical reactions of this process is oxygen evolution reaction (OER). However, this reaction is kinetically sluggish due to a complex multistep four-electron oxidation[1-5]. To reach a desirable current density of 10 mA cm^{-2}, which is a metric associated with solar fuel synthesis, a considerable overpotential (η) relative to thermodynamic potential of the reaction is required, but will hinder the large-scale electrochemical water splitting[3,4]. Currently, RuO_2 and IrO_2 are among the most active OER catalysts, however, their unacceptable cost and low abundance severely restrict their large-scale applications[5,6]. Therefore, it is of great technological and scientific significance to pursue highly efficient alternatives on the basis of earth-abundant nonprecious materials.

Transition-metal oxides and their derivatives have received much attention because of their earth-abundant reserves, low cost, environment-friendly features and remarkable OER activities[7-23]. Specially, cobalt oxides, such as layered $LiCoO_2$ (refs 11,12), Co-oxyhydroxides (refs 13,14), spinel Co_3O_4 (refs 15–17), perovskite $Ba_{0.5}Sr_{0.5}Co_{0.8}Fe_{0.2}O_{3-\delta}$ (BSCF)[18] and $PrBaCo_2O_{5+\delta}$ (ref. 19), have been explored as potential OER catalysts due to their high activities comparable to and even better than the precious metal oxides. Theoretical and experimental works have shown that the OER activity is intrinsically related to the electronic structure of Co ions, including oxidation state and spin configuration, which enlightens the rational design of optimal catalysts[7-21]. For example, Lu et al.[12] recently reported that the OER activity of $LiCoO_2$ was remarkably enhanced by tuning the Co oxidation state via electrochemical delithiation process. More interestingly, for perovskite transition-metal oxides, Shao-Horn and co-workers[18] demonstrated the direct dependence of OER activity on the e_g orbital filling of the transition-metal ions, and that the oxide BSCF with $e_g^{\sim 1.2}$ configuration exhibited the highest OER activity. The performance of the BSCF was found to be nearly identical to IrO_2 in terms of catalytic activity. However, this Co-based oxide undergoes surface amorphization after long-term potential cycles under OER conditions[22]. Therefore, substantial progress is still needed to develop perovskite-type OER catalysts with improved activity and stability. In this respect, Shao-Horn's principle highlights that the optimization of e_g filling close to 1.2 should be an alternative strategy to develop the transition-metal oxides as the effective OER catalysts. Practically, a recent study by Zhu et al.[23] supported this principle, where an improved OER activity was realized through adjusting the e_g filling to ~ 1.2 with partial substitution of Co by Nb in $SrCo_{0.8}Fe_{0.2}O_{3-\delta}$ (ref. 23).

In this work, we present a facile method to modify the electronic structure of Co ions by varying the particle size for the improvement in the OER activity. We focus on the perovskite cobaltite $LaCoO_3$ (LCO), which is well-known for its unique thermally-driven transition of Co^{3+} ions from low spin (LS: $t_{2g}^6 e_g^0$) at low temperatures to higher spin state with e_g orbital configuration of $e_g^{\sim 1.0}$ at room temperature[18,24-31]. This compound was reported to exhibit reasonable OER activity but much less than BSCF[18]. Here, by reducing the particle size, the e_g filling is successfully increased from unity to close to the optimization configuration of ~ 1.2. As a consequence, the OER activity of the 80-nm LCO is higher than those of other sized samples as well as the bulk, and comparable to those of the reported cobalt oxides with $e_g^{\sim 1.2}$ filling, which enables the nanosized LCO to be applicable as a promising OER catalyst.

Results

Crystal structures of the bulk and nanosized LCO. The LCO samples were prepared by a sol–gel method[32,33]. The precursory powders derived from the gel were annealed at 600, 700 and 800 °C

for 6 h to produce the LCO nanoparticles with the particle size of about 60, 80 and 200 nm (ref. 32), respectively, as well as at 1,000 °C for 12 h to the bulk sample with the particle size of about 0.5–1 μm (Supplementary Fig. 1). A representative transmission electron microscopy (TEM) image for the 700 °C annealing sample is shown in Fig. 1a. The high-resolution TEM images and the selective area electron diffraction patterns reveal a single-crystal structure of small LCO particles with a high crystallinity (Supplementary Fig. 2). The X-ray diffraction patterns (Fig. 1b and Supplementary Fig. 3) reveal that all the samples take a rhombohedral structure with R $\bar{3}c$ space group (Fig. 1c). The structural parameters obtained from the Rietveld refinements on the diffraction data are given in Supplementary Table 1. As the particle size is reduced, the unit cell is found to be expanded. Specially, the bond length of Co–O exhibits an obvious increase (Fig. 1d).

Spin structures of the bulk and nanosized LCO. The temperature-dependent magnetizations were measured with a magnetic field of $H = 1$ kOe under field-cooling procedures for all the samples (Supplementary Fig. 4a) to study the spin structures of Co ions controlled by the particle size. Above 150 K, the susceptibilities derived from the magnetizations ($\chi = M/H$) obey a paramagnetic Curie–Weiss law: $\chi = C/(T - \Theta)$, where C is Curie constant, and Θ is Curie–Weiss temperature. From the fitting results (Fig. 2a), an effective magnetic moment μ_{eff} can be calculated through $\mu_{eff} = \sqrt{8C}\ \mu_B$ (Supplementary Fig. 4b). For the bulk LCO, although the exact nature of whether the higher spin state of Co^{3+} ions at room temperature is intermediate-spin (IS: $t_{2g}^5 e_g^1$) state or a mixture of LS and high spin (HS: $t_{2g}^4 e_g^2$) states was controversial in the past decades[24-27], a large number of recent theoretical and experimental studies reveal that the mixture of LS and HS states is more favourable[28-31]. Here, the calculated μ_{eff} of 3.48 μ_B for the bulk sample is well consistent with those values reported for the polycrystalline bulk LCO, which corresponds to the Co^{3+} ions in 50% HS + 50% LS states as well as the e_g filling of ~ 1.0 (refs 25, 28–31). For the nanosized LCO, μ_{eff} shows a gradual increase with the decrease of the particle size, suggesting that the spin state of partial Co ions transmits from LS to HS state. Using the calculated μ_{eff}, the spin states are estimated to be 55% HS + 45% LS, 60.5% HS + 39.5% LS and 63.7% HS + 36.3% LS for the 200, 80 and 60 nm samples (Supplementary Note 1 and Supplementary Table 2), meaning that about 5, 10.5 and 13.7% Co^{3+} ions in LS state change to be in HS state, respectively. As shown in Fig. 2b, the corresponding e_g filling is about 1.1, 1.2 and 1.27 for the nanosized LCO, respectively. It is worthwhile to emphasize that by reducing the particle size to about 80 nm, we successfully tune the e_g filling from unity to the optimization value of 1.2 expected by Shao-Horn's principle.

To further confirm the spin-state transition and to explore its possible origin, the electron energy loss spectroscopy (EELS) analyses on the LCO nanoparticles were performed on the scanning TEM. Figure 2c,d shows the representative EELS spectra at Co L- and O K-edges from the centre and edge of the 80 nm nanoparticle, which are sensitive to the electronic structure from the core (bulk) and shell (surface), respectively[34,35]. For the Co L-edge spectra, no noticeable changes in the L_3/L_2 ratio between the bulk and surface were found, suggesting that the oxidation state of Co ions remained unchanged[35-39]. For the O K-edge spectra, three characteristic peaks near the edge onset, labelled a, b and c, were observed. The prepeak a, b and c were assigned to the hybridization of O 2p with Co 3d, La 5d and Co 4sp orbitals, respectively[36-39]. Compared with that from the centre position, the spectrum from the edge shows an obvious reduction in the intensity of the prepeak a. Similar results are also found in the
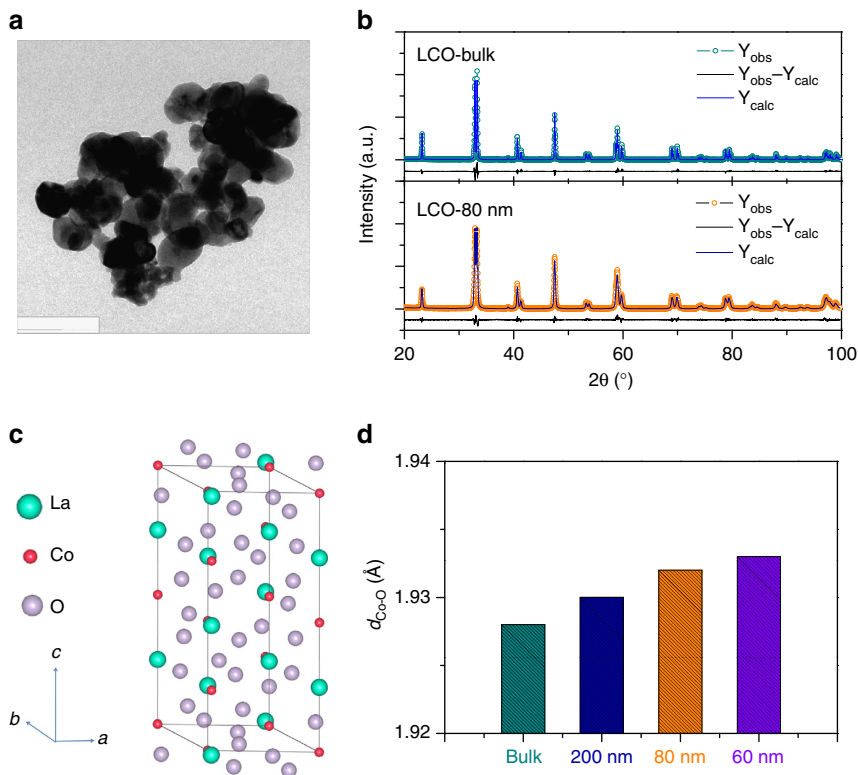
Figure 1 | TEM image and crystal structure analyses of the bulk and nanosized LCO. (**a**) TEM image for the 80 nm LCO. (**b**) X-ray diffraction patterns for bulk and 80 nm LCO together with the Rietveld refined results. (**c**) LCO crystal structure. (**d**) The length of Co–O bond for the bulk and nanosized LCO. Scale bar, 180 nm.
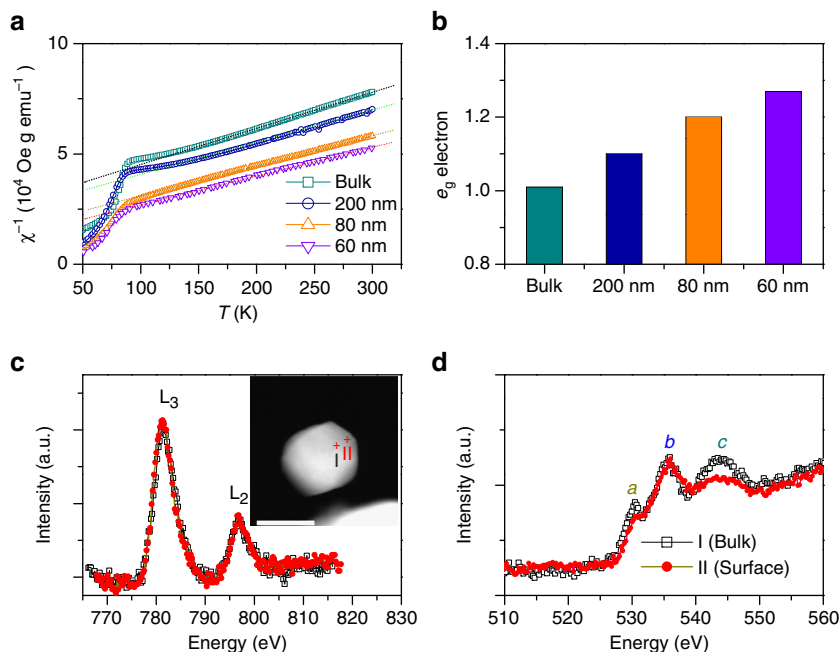

Figure 2 | Spin structure analyses of the bulk and nanosized LCO. (**a**) The temperature dependence inverse susceptibilities for all the LCO samples. The dotted lines are the fitting results by a Curie–Weiss law. (**b**) The corresponding e_g filling. (**c,d**) Representative EELS spectra of the 80 nm LCO at Co L-edge and O K-edge, respectively. The inset corresponds to the representative position of EELS acquisition. Scale bar, 50 nm.

other nanoparticles (Supplementary Fig. 5). This reduction is generally attributed to the formation of oxygen vacancy or the weakening of Co 3d–O 2p hybridization[36–39]. Since the Co L-edge spectra revealed no change in the Co oxidation state, the

formation of oxygen vacancies can be excluded. Thus, the modification of O K-edge would originate from the change of the Co 3d–O 2p hybridization. Previous works have been widely reported that the spin-state transition of Co^{3+} ions in the LCO

can significantly modify the hybridization of Co $3d$–O $2p$ orbitals and then the intensity of the prepeak a (refs 35–39). In the LS configuration, the $3d$ e_g levels of Co^{3+} ions are completely empty, allowing the electrons from the filled O $2p$ levels to be shared with Co e_g orbitals, and accordingly creating O $2p$ holes. Thus, the hybridization of Co $3d$ with the O $2p$ states promotes electron transitions between $1s$ and the unfilled O $2p$ state, resulting in the prepeak a of the O K-edge. However, as a HS state of the Co^{3+} ions emerges, the e_g orbitals are increasingly occupied, which prevents the charge transfer and weakens the hybridization of O $2p$ with Co $3d$ orbitals, resulting in the decreased intensity of the prepeak a (refs 36–39). Therefore, the decrease in the intensity of the prepeak a at the surface confirms the existence of surface spin-state transitions in the nanosized LCO.

We proposed a mechanism to explain the presence of surface spin-state transitions of Co^{3+} ions where the modified crystal field splitting of Co $3d$ orbital at the surface favors the Co^{3+} ions to be in HS states, which has also been reported in nanosized stoichiometric $LiCoO_2$ (ref 40). Assuming that Co^{3+} ions within surface layers are all transited to be in HS state, we can give a rough estimate of the e_g filling for the nanosized LCO on the basis of a simple core-shell model (Supplementary Note 2 and Supplementary Fig. 6). For nanosized perovskite oxides with the particle size ranging from tens to hundreds of nanometres, the surface layers are usually reported to be about 2–5 nm in the thickness[41–44]. Taking the thickness of 3 nm (see Supplementary Fig. 2), the estimated volume fractions of the surface layer are about 8.7, 20.8 and 27.1% for the 200, 80 and 60 nm LCO, respectively. Consequently, the increased fractions of the HS Co^{3+} ions are 4.4, 10.4 and 13.6%, which means that the e_g fillings are increased to be about 1.09, 1.21 and 1.27, respectively. These values are well consistent with those obtained from the magnetizations, further supporting that the tuning of e_g filling by the size reduction originates from the surface spin-state transition. In addition, since the radii of Co^{3+} ions increases when their spin state changes from LS to HS, the presence of this transition is also confirmed by the crystal structure data, where the expansion of the unit cell and the increase of Co–O length under decreasing the particle size are found (Supplementary Table 1 and Fig. 1d).

OER activities of the bulk and nanosized LCO. To shed light on the role that the surface spin-state transition plays in the OER activity for the LCO, the electrochemical measurements were carried out in O_2-saturated 0.1 M KOH solutions using a standard three-electrode system. Figure 3a shows the iR-corrected polarization curves for all the samples, where the LCO nanoparticles exhibited smaller onset overpotentials than that of the bulk (~ 0.37 V). In particular, the smallest onset overpotential of ~ 0.32 V was observed in the 80 nm LCO. Similarly, the overpotential η required to achieve a current density of 10 mA cm^{-2} was also reduced from 0.62 V for the bulk to 0.54, 0.49 and 0.55 V as the particle size decreased to about 200, 80 and 60 nm, respectively. Figure 3b plots the dependence of mass activity at $\eta = 0.49$ V on the e_g filling. As the e_g filling approached the optimal configuration of ~ 1.2, the current density reached the largest value, which was about 4.3 times larger than that of the bulk. Moreover, the corresponding Tafel plots (Fig. 3d) also reveal that the 80 nm LCO possessed the smallest Tafel slope of ~ 69 mV dec^{-1}, much smaller than that of the bulk (~ 102 mV dec^{-1}). This large reduction suggests that the rate-determining step tends to change from the –OH adsorption to the O–OH formation[18,45,46]. In addition, the preliminary stability tests for the bulk and 80 nm LCO under a constant galvanostatic current of 10 A g^{-1} (Supplementary Fig. 7) also demonstrate that the 80 nm sample exhibited better stability than the bulk. As revealed by Co $2p$ X-ray photoelectron spectra of the 80 nm LCO before and after the electrolysis (Supplementary Fig. 8), no visible changes for the Co $2p$ spectra were found during the electrolysis, suggesting that the electronic state of the Co ions may remain unchanged. All of the above results clearly indicate that the OER
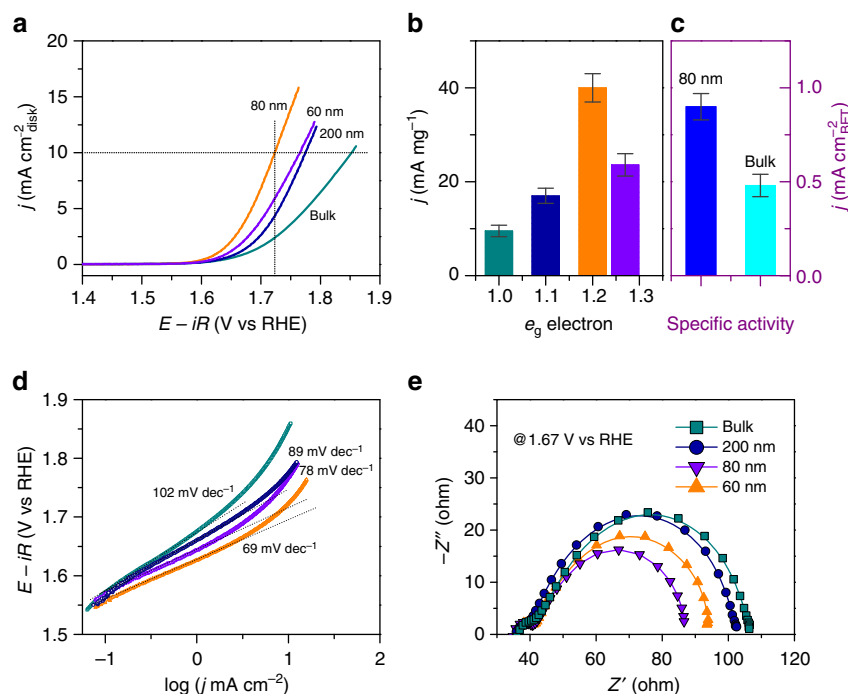

Figure 3 | OER activities of the bulk and nanosized LCO. (**a**) Polarization curves of the bulk and nanosized LCO. (**b**) Mass and (**c**) special activities at $\eta = 0.49$ V. (**d**) Tafel plots for the bulk and nanosized LCO. (**e**) Nyquist plots for the bulk and nanosized LCO. Error bars represent the s.d. from at least three independent measurements.

Table 1 | Comparison of OER activity for different catalysts.

Catalyst	Onset overpotential (V vs RHE)	η @ j = 10 mA cm^{-2} (V)	Tafel slope (mV dec^{-1})	e_g filling	Ref.
LCO-bulk	0.37	0.62	102	$e_g^{\sim 1.0}$	This work
LCO-80 nm	0.33	0.49	69	$e_g^{\sim 1.2}$	This work
$Ba_{0.5}Sr_{0.5}Co_{0.8}Fe_{0.2}O_{3-\delta}$	—	0.49	84	$e_g^{\sim 1.2}$	(ref. 21)
$Ba_{0.5}Sr_{0.5}Co_{0.8}Fe_{0.2}O_{3-\delta}$	0.30	0.50	94	$e_g^{\sim 1.2}$	(ref. 23)
$SrCo_{0.9}Ti_{0.1}O_{3-\delta}$	—	0.51	88	$e_g^{\sim 1.16}$	(ref. 21)
$SrNb_{0.1}Co_{0.7}Fe_{0.2}O_{3-\delta}$	0.30	0.50	76	$e_g^{\sim 1.2}$	(ref. 23)

OER, oxygen evolution reaction.

activity of the LCO is successfully modified by controlling the particle size. As the particle size is reduced to about 80 nm with the $e_g^{\sim 1.2}$ configuration, the activity is significantly enhanced.

The origin of the enhanced OER activity. As the sample size is reduced, the enhanced mass catalytic activity towards the OER is largely ascribed to the increase of the surface area. Such scenarios were reported in various Co-based oxides such as BSCF[18], $SrNd_{0.1}Co_{0.7}Fe_{0.2}O_{3-\delta}$ (ref. 23) and $NiCo_2O_4$ (ref. 47). However, in those cases, the size reduction leaded to a large decrease in the specific OER activities, that is, the normalized activities by the surface area. Since the specific activity reflects the intrinsic activity of the catalysis, this decrease indicates that intrinsic OER activity was deteriorated by reducing the sample size for those oxides. To clarify whether the enhancement of the OER activity in our LCO nanoparticles is intrinsic, the specific activities are further calculated on the basis of two types of surface areas, the Brunauer-Emmett-Teller (BET) surface areas and the electrochemically active surface areas, obtained by means of the gas desorption (Supplementary Fig. 9) and electrochemical double-layer capacitance measurements (Supplementary Fig. 10 and Supplementary Note 3), respectively. The specific activities at η = 0.49 V normalized by the surface areas exhibit similar dependences on the e_g filling to the mass activity (Supplementary Fig. 11). Compared with the bulk, the 80 nm sample is still 1.8 times more active in the specific activity normalized by the BET area (Fig. 3c), which strongly suggests that the increased number of active sites from the surface areas may be not the main contribution to the significant enhancement of the OER activity. The improved performance would be mainly attributed to the increased reactivity of the active sites due to the spin-state transition of Co^{3+} ions at surfaces. When the e_g filling of Co^{3+} ions increases from about 1.0 to 1.2, the electron occupancy of the Co 3d–O 2p σ* band increases with the elongation of the length of Co–O bond as shown in Figs 1d and 2d. Thus, the hybridization of Co 3d–O 2p orbitals and the strength of Co–O bond become weaker, which leads to a less surface coverage by –OH groups on the active sites and thereby facilitates the formation of –OOH species[45,46]. As a result, the Tafel slope is reduced and the OER activity is improved. On the other hand, it has been generally demonstrated that H_2O molecules are initially adsorbed onto the surface of catalysts during the OER process[13,18,45]. Consequently, the adsorption energy of H_2O onto the active site plays a crucial role in the OER activity. Our density functional theory (DFT) calculations on the adsorption energy of H_2O onto the surface Co ions in different spin states reveal that the surface Co ions being in HS state are more favourable for adsorbing H_2O molecular (Supplementary Fig. 12 and Supplementary Table 3), well consistent with the improvement of the OER activity by reducing the particle size to 80 nm. However, it is worthwhile to note that as the particle size is further reduced to about 60 nm the activity decreases again, which cannot be explained by the above factors. We propose that the excessive e_g occupancy (>1.2) of the Co^{3+} ions in this sample would make the charge transfer ability lower. As such, when the two neighboured Co ions in Co–O–Co network are both in

HS state, the half-filling of e_g orbitals tends to prevent the charge transfer. To confirm this point, the electrochemical impedance spectroscopy experiments have been carried out. As shown in Fig. 3e, the Nyquist plots reveal that the charge transfer resistance gradually decreases with the reduction of the particle size to 80 nm, while increases again as the size is further reduced to 60 nm. Therefore, we conclude that the modifications of the Co–O binding strength and the charge transfer ability associated with the surface spin-state transition in the LCO are responsible for the size-dependent OER activity.

Finally, we compared the OER activity of our LCO samples with those of the recently reported Co-based perovskite oxides with the optimal configuration of $e_g^{\sim 1.2}$. As illustrated in Table 1, it is interesting to find that the 80 nm LCO exhibits a well comparable activity with those well-known catalysts, which further consolidates Shao-Horn's principle and suggests that tuning the spin state can provide an effective strategy to improve the OER activity.

Discussion

In summary, we highlight an effective strategy to engineer the electronic configuration of perovskite cobalt oxide for the development of high active electrocatalysts. By reducing the particle size to about 80 nm, the spin filling of Co ions in LCO is successfully tuned from unity (bulk) to near the optimization configuration of ~ 1.2 expected by Shao-Horn's principle. Through X-ray diffraction, magnetic measurements and EELS analysis, we confirm that this modification originates from the size-induced spin-state transition of Co^{3+} ions from LS to HS state. Consequently, the nanosized sample exhibits an improved OER activity with lower overpotential, smaller Tafel slope and better stability compared with the bulk. More interestingly, the performance of the 80 nm LCO can be comparable with those of the reported cobalt oxides with $e_g^{\sim 1.2}$ filling, suggesting that the LCO in this nanosized form can serve as a promising OER catalyst. Our work paves the way for the rational design of high-efficient OER catalysts.

Methods

Synthesis and characterization. $La(NO_3)_3 \cdot 6H_2O$ and $Co(NO_3)_2 \cdot 6H_2O$ were dissolved in deionized water, followed by the addition of a mixture of citric acid and ethylene glycol. Subsequently, the obtained transparent solution was slowly evaporated to get a gel, which was decomposed at about 400 °C for 4 h to result in dark brown powders. The precursor powders were further annealed at 600, 700 and 800 °C for 6 h to produce LCO nanoparticles with different particle sizes, and at 1,000 °C for 12 h to the bulk sample. The phase purity and crystal structure of the samples were determined by X-ray diffraction at room temperature on a Rigaku TTR-III diffractometer using Cu K_a radiation (λ = 1.5418 Å). The field emission SEM and TEM images were obtained on a JEOL-2010 SEM and a JEM-2100F TEM, respectively. The HRTEM images and the EELS analyses were performed on a JEOL JEM-ARM200F TEM/scanning TEM with a spherical aberration corrector. The magnetic measurements were carried out with a MPMS SQUID magnet-ometer. The nitrogen adsorption − desorption isotherms were conducted on a Micromeritics ASAP 2000 system at 77 K. X-ray photoelectron spectra were carried out on an ESCALAB 250 X-ray photonelectron spectrometer with Al Kα as the excitation source.

Electrochemical measurements. The electrochemical tests were performed in O_2-saturated 0.1 M KOH with a conventional three-electrode on the CHI660B electrochemical station. Saturated Ag/AgCl and platinum wires were used as the reference and the counter electrodes, respectively. The reference electrode was calibrated with respect to the reversible hydrogen electrode (RHE), which was carried out in the high-purity hydrogen saturated electrolyte with a Pt wire as the working electrode. Cyclic voltammetry was run at a sweep rate of $1\,mV\,s^{-1}$. The average of the two potentials at which the current crossed zero was taken to be the thermodynamic potential for the hydrogen electrode reactions. In 0.1 M KOH, $E_{RHE} = E_{Ag/AgCl} + 0.964\,V$. To prepare the working electrode, 3.5 mg of electrocatalyst and 20 μl of 5 wt% Nafion solutions were dispersed in 1 ml ethanol with sonication for at least 30 min to form a mixted ink. Then, 5 μl of this solution was drop-casted onto a 3 mm in diameter glassy carbon electrode and dried naturally, yielding a catalyst loading of $0.25\,mg\,cm^{-2}$. Linear sweeping voltammograms were obtained at a scan rate of $5\,mV\,s^{-1}$. The potentials are corrected to compensate for the effect of solution resistance, which were calculated by the following equation: $E_{iR-corrected} = E - iR$, where i is the current, and R is the uncompensated ohmic electrolyte resistance ($\sim36\,\Omega$) measured via high frequency ac impedance in O_2-saturated 0.1 M KOH. The polarization curves were replotted as overpotential (η) vs log current (log j) to get Tafel plots for quantification of the OER activities of investigated catalysts. Electrochemical impedance spectroscopy were conducted with AC voltage with 5 mV amplitude at the potential of 1.67 V vs RHE within the frequency range from 100 KHz to 100 mHz. Durablity test was performed at room temperature under a constant galvanostatic current of $10\,A\,g^{-1}$. Error bars represented s.d. from at least three independent measurements.

DFT calculations. DFT + U calculations with the Vienna *ab initio* simulation package[48] for a water molecule adsorbed on (001) surface of LCO with LS and HS state on Co^{3+} ions were performed to study the influence on adsorption energy of water molecule with different spin states of Co^{3+} ions. A slab model consisting of eight atom-layers ($La_{16}Co_{16}O_{48}$) was used to simulate the (001) surface with two terminations. In calculations, an effective U of 3.4 eV was added on Co $3d$ orbital, the plane wave energy cut-off was set to 400 eV, and a $2 \times 2 \times 1$ Monkhorst–Pack k-point mesh was used. During geometry optimization, converge criteria were 10^{-5} eV for energy and $0.05\,eV\,Å^{-1}$ for force. The LS of Co^{3+} was not obtained on CoO_2 terminated (001) surface, since surface Co^{3+} was in a five-coordinated structure and turns into HS during the calculation even though it was set to LS initially.

Data availability. The data that support the findings of this study are available from the corresponding author on request.

References

1. Gray, H. B. Powering the planet with solar fuel. *Nat. Chem.* **1**, 7 (2009).
2. Lewis, N. S. & Nocera, D. G. Powering the planet: chemical challenges in solar energy utilization. *Proc. Natl Acad. Sci. USA* **103**, 15729–15735 (2007).
3. Cook, T. R. *et al.* Solar energy supply and storage for the legacy and nonlegacy worlds. *Chem. Rev.* **110**, 6474–6502 (2010).
4. Walter, M. G. *et al.* Solar water splitting cells. *Chem. Rev.* **110**, 6446–6473 (2010).
5. Jiao, Y., Zheng, Y., Jaroniec, M. & Qiao, S. Z. Design of electrocatalysts for oxygen and hydrogen-involving energy conversion reactions. *Chem. Soc. Rev.* **44**, 2060–2086 (2015).
6. Lee, Y., Suntivich, J., May, K. J., Perry, E. E. & Shao-Horn, Y. Synthesis and activities of rutile IrO_2 and RuO_2 nanoparticles for oxygen evolution in acid and alkaline solutions. *J. Phys. Chem. Lett.* **3**, 399–404 (2012).
7. Yuan, C. Z., Wu, H. B., Xie, Y. & Lou, X. W. Mixed transition metal oxides: design, controllable synthesis and energy-related applications. *Angew. Chem. Int. Ed.* **53**, 1488–1504 (2014).
8. Wang, H. *et al.* Bifunctional non-noble metal oxide nanoparticle electrocatalysts through lithium-induced conversion for overall water splitting. *Nat. Commun.* **6**, 7261 (2015).
9. Hong, W. T. *et al.* Toward the rational design of non-precious transition metal oxides for oxygen electrocatalysis. *Energy Environ. Sci.* **8**, 1404–1427 (2015).
10. Kim, J. M., Yin, X., Tsao, K.-C., Fang, S. H. & Yang, H. $A_2B_2O_5$ as oxygen deficient perovskite electrocatalyst for oxygen evolution reaction. *J. Am. Chem. Soc.* **136**, 14646–14649 (2014).
11. Maiyalagan, T., Jarvis, K. A., Therese, S., Ferreira, P. J. & Manthiram, A. Spinel-type lithium cobalt oxide as a bifunctional electrocatalyst for the oxygen evolution and oxygen reduction reactions. *Nat. Commun.* **5**, 3949 (2014).
12. Lu, Z. *et al.* Electrochemical tuning of layered lithium transition metal oxides for improvement of oxygen evolution reaction. *Nat. Commun.* **5**, 5345 (2014).
13. Huang, J. H. *et al.* CoOOH nanosheets with high mass activity for water oxidation. *Angew. Chem. Int. Ed.* **54**, 8722–8727 (2015).
14. Song, F. & Hu, X. L. Exfoliation of layered double hydroxides for enhanced oxygen evolution catalysis. *Nat. Commun.* **5**, 4477 (2014).
15. Ma, T. Y., Dai, S., Jaroniec, M. & Qiao, S. Z. Metal-organic framework-derived hybrid Co_3O_4-carbon porous nanowire arrays as reversible oxygen evolution electrodes. *J. Am. Chem. Soc.* **136**, 13925–13931 (2014).
16. Hu, H., Guan, B. Y., Xia, B. Y. & Lou, X. W. Designed formation of Co_3O_4/$NiCo_2O_4$ double-shelled nanocages with enhanced pseudocapacitive and electrocatalytic properties. *J. Am. Chem. Soc.* **137**, 5590–5595 (2015).
17. Deng, X. H. & Tüysüz, H. R. Cobalt-oxide-based materials as water oxidation catalyst: recent progress and challenges. *ACS Catal.* **4**, 3701–3714 (2014).
18. Suntivich, J., May, K. J., Gasteiger, H. A., Goodenough, J. B. & Shao-Horn, Y. A perovskite oxide optimized for oxygen evolution catalysis from molecular orbital principles. *Science* **334**, 1383–1385 (2011).
19. Grimaud, A. *et al.* Double perovskites as a family of highly active catalysts for oxygen evolution in alkaline solution. *Nat. Commun.* **4**, 2439 (2013).
20. Kanan, M. W. *et al.* Structure and valency of a cobalt-phosphate water oxidation catalyst determined by *in situ* X-ray spectroscopy. *J. Am. Chem. Soc.* **132**, 13692–13701 (2010).
21. Su, C. *et al.* $SrCo_{0.9}Ti_{0.1}O_{3-\delta}$ as a new electrocatalyst for the oxygen evolution reaction in alkaline electrolyte with stable performance. *ACS Appl. Mater. Interfaces* **7**, 17663–17670 (2015).
22. Risch, M. *et al.* Structural changes of cobalt-based perovskites upon water oxidation investigated by EXAFS. *J. Phys. Chem. C* **117**, 8626–8635 (2013).
23. Zhu, Y. *et al.* $SrNb_{0.1}Co_{0.7}Fe_{0.2}O_{3-\delta}$ perovskite as a next-generation electrocatalyst for oxygen evolution in alkaline solution. *Angew. Chem. Int. Ed.* **54**, 3897–3901 (2015).
24. Raccah, P. M. & Goodenough, J. B. First-order localized-electron $\leftrightarrows$ collective-electron transition in $LaCoO_3$. *Phys. Rev.* **155**, 932 (1967).
25. Señarís-Rodríguez, M. A. & Goodenough, J. B. $LaCoO_3$ revisited. *J. Solid State Chem.* **116**, 224–231 (1995).
26. Korotin, M. A. *et al.* Intermediate-spin state and properties of $LaCoO_3$. *Phys. Rev. B* **54**, 5309 (1996).
27. Zobel, C. *et al.* Evidence for a low-spin to intermediate-spin state transition in $LaCoO_3$. *Phys. Rev. B* **66**, 020402 (2002).
28. Phelan, D. *et al.* Nanomagnetic droplets and implications to orbital ordering in $La_{1-x}Sr_xCoO_3$. *Phys. Rev. Lett.* **96**, 027201 (2006).
29. Hoch, M. J. R. *et al.* Diamagnetic to paramagnetic transition in $LaCoO_3$. *Phys. Rev. B* **79**, 214421 (2009).
30. Křápek, V. *et al.* Spin state transition and covalent bonding in $LaCoO_3$. *Phys. Rev. B* **86**, 195104 (2012).
31. Karolak, M. *et al.* Correlation-driven charge and spin fluctuations in $LaCoO_3$. *Phys. Rev. Lett.* **115**, 046401 (2015).
32. Zhou, S. M. *et al.* Size-dependent structural and magnetic properties of $LaCoO_3$ nanoparticles. *J. Phys. Chem. C* **113**, 13522–13526 (2009).
33. Zhou, S. M. *et al.* Ferromagnetism in $LaCoO_3$ nanoparticles. *Phys. Rev. B* **76**, 172407 (2007).
34. Rossell, M. D. *et al.* Direct evidence of surface reduction in monoclinic $BiVO_4$. *Chem. Mater.* **27**, 3593–3600 (2015).
35. Han, B. H. *et al.* Role of $LiCoO_2$ surface terminations in oxygen reduction and evolution kinetics. *J. Phys. Chem. Lett.* **6**, 1357–1362 (2015).
36. Gazquez, J. *et al.* Atomic-resolution imaging of spin-state superlattices in nanopockets within cobaltite thin films. *Nano Lett.* **11**, 973–976 (2011).
37. Kwon, J. H. *et al.* Nanoscale spin-state ordering in $LaCoO_3$ epitaxial thin films. *Chem. Mater.* **26**, 2496–2501 (2014).
38. Lan, Q. Q. *et al.* Correlation between magnetism and 'dark stripes' in strained $La_{1-x}Sr_xCoO_3$ epitaxial films ($0 \leq x \leq 0.1$). *Appl. Phys. Lett.* **107**, 242404 (2015).
39. Klie, R. F. *et al.* Direct measurement of the low-temperature spin-state transition in $LaCoO_3$. *Phys. Rev. Lett.* **99**, 047203 (2007).
40. Qian, D. *et al.* Electronic spin transition in nanosize stoichiometric lithium cobalt oxide. *J. Am. Chem. Soc.* **134**, 6096–6099 (2012).
41. Zhou, S. M. *et al.* Magnetic phase diagram of nanosized half-doped manganites: role of size reduction. *Daton Trans.* **41**, 7109–7114 (2012).
42. Curiale, J. *et al.* Magnetic dead layer in ferromagnetic manganite nanoparticles. *Appl. Phys. Lett.* **95**, 043106 (2009).
43. Wang, Y. & Fan, H. J. Low-field magnetoresistance effect in core–shell structured $La_{0.7}Sr_{0.3}CoO_3$ nanoparticles. *Small* **8**, 1060–1065 (2012).
44. Vasseur, S. *et al.* Lanthanum manganese perovskite nanoparticles as possible *in vivo* mediators for magnetic hyperthermia. *J. Magn. Magn. Mater.* **302**, 315–320 (2006).
45. Wang, H. Y. *et al.* In operando identification of geometrical-site-dependent water oxidation activity of spinel Co_3O_4. *J. Am. Chem. Soc.* **138**, 36–39 (2016).
46. Malkhandi, S. *et al.* Design insights for tuning the electrocatalytic activity of perovskite oxides for the oxygen evolution reaction. *J. Phys. Chem. C* **119**, 8004–8013 (2015).
47. Bao, J. *et al.* Ultrathin spinel-structured nanosheets rich in oxygen deficiencies for enhanced electrocatalytic water oxidation. *Angew. Chem. Int. Ed.* **127**, 7507–7512 (2015).
48. Kresse, G. & Furthmuller, J. Efficient iterative schemes for *ab initio* total-energy calculations using a plane-wave basis set. *Phys. Rev. B* **54**, 11169 (1996).

Acknowledgements

Author contributions

S.Z., Z.H. and J.Ze. designed the studies and wrote the paper. X.M., X.Z., C.M. and J.Zh. performed most of the experiments. Y.Q. and Z.H. carried out DFT calculations. S.Z., C.M., Z.H., L.S. and J.Ze. performed data analysis. All authors discussed the results and commented on the manuscript.

Additional information

Supplementary Information accompanies this paper at http://www.nature.com/naturecommunications

Competing financial interests: The authors declare no competing financial interests.

Reprints and permission information is available online at http://npg.nature.com/reprintsandpermissions/

How to cite this article: Zhou, S. *et al.* Engineering electrocatalytic activity in nanosized perovskite cobaltite through surface spin-state transition. *Nat. Commun.* 7:11510 doi: 10.1038/ncomms11510 (2016).